Diffuse Reflectance Infrared Studies of the Reaction of Synthetic Sea Salt Mixtures with NO_2: A Key Role for Hydrates in the Kinetics and Mechanism

Sarka Langer, R. Sean Pemberton, and Barbara J. Finlayson-Pitts*

Department of Chemistry, University of California, Irvine, California 92697-2025

Received: July 16, 1996; In Final Form: October 23, 1996[⊗]

The heterogeneous reactions of oxides of nitrogen with NaCl as a model for sea salt particles have been the focus of many studies, due to their potential to act as precursors to atomic halogens in the troposphere. While a great deal has been learned about the kinetics and mechanisms of NaCl reactions, it is not clear how well this extrapolates to the complex mixture of inorganics found in sea salt. We report here diffuse reflectance infrared Fourier transform spectrometry (DRIFTS) studies in which nitrate formation on the salt surface is followed with time during the reaction of gaseous NO_2 with synthetic sea salt at 298 K in the presence of either He or air as the carrier gas. The infrared bands due to surface nitrate formed during the reaction of NO_2 are shown to be similar to those from the reaction of $MgCl_2 \cdot 6H_2O$, a major hydrate in the mixture which was used as a surrogate for all of the crystalline hydrates. Significant amounts of surface-adsorbed water are generated in the reaction of synthetic sea salt with NO_2 in air, which appears at least in part to be due to liberation of bound water of hydration in the crystalline hydrates. The reaction order with respect to NO_2 is (1.8 ± 0.2) (2σ) when the reaction of the synthetic sea salt is carried out in He but only (1.2 ± 0.2) (2σ) when air is used as the carrier gas. For comparison, the reaction order for the NO_2−NaCl reaction was reexamined and found to be (1.8 ± 0.3) (2σ) in He and (1.6 ± 0.3) (2σ) in air, in agreement with previous work[19] using this technique. It is assumed for slopes ≥ 1.6 that N_2O_4 is the reacting species for the purpose of expressing the kinetics in the usual form of reaction probabilities. For the N_2O_4−NaCl reactions in He and air, and for the N_2O_4−synthetic sea salt reaction in He, the reaction probabilities are similar ($\sim 10^{-4}$). The reaction of synthetic sea salt with NO_2 in the presence of air is treated in terms of a first-order reaction with NO_2 being the reactive species, which gives a reaction probability for the NO_2−synthetic sea salt reaction of $\sim 10^{-8}$. The atmospheric implications are discussed.

Introduction

The kinetics and mechanisms of the reactions of gases with solids in the atmosphere is an area of current intense interest. For example, reactions of sea salt particles and their components have received increased attention as potential sources of chlorine and bromine atoms in the troposphere.[1−5] Airborne sea salt particles are released to the atmosphere from spray formed by wave action in the surface layer of seawater.[6] These particles are expected to exist primarily as concentrated salt solutions at the high relative humidities found in the marine boundary layer. However, as they are transported to drier areas such as inland or to higher altitudes, the water will evaporate, leaving suspended solid salt particles. These can react with various gases, in particular various oxides of nitrogen, potentially contributing to the chemistry of the troposphere.

Since NaCl is the major component of sea salt particles, it has been used in many past studies as a model. This has the additional advantage of allowing relevant reactions to be studied in a well-defined system since NaCl of high purity is readily available as small crystals, powders, and large single crystals with exposed (100) or (111) faces. The reactions studied to date[7−30] include

$$NaCl(s) + HNO_3(g) \rightarrow NaNO_3(s) + HCl(g) \quad (1)$$

$$NaCl(s) + 2NO_2(g) \rightarrow NaNO_3(s) + ClNO(g) \quad (2)$$

$$NaCl(s) + N_2O_5(g) \rightarrow NaNO_3(s) + ClNO_2(g) \quad (3)$$

$$NaCl(s) + ClONO_2(g) \rightarrow NaNO_3(s) + Cl_2(g) \quad (4)$$

Accurate measurements of the kinetics of reaction 1 compared to reactions 2−4 and understanding what controls the kinetics at a molecular level are important for assessing the atmospheric importance of the reactions of sea salt particles. Reactions 2−4 all generate photochemically active chlorine compounds which will dissociate to form highly reactive chlorine atoms. In the troposphere where significant concentrations of organics are present globally, atomic chlorine reacts to form alkyl (R) radicals:

$$Cl + RH \rightarrow R + HCl \quad (5)$$

The alkyl radicals then add O_2 to form RO_2, which can oxidize NO to NO_2 and form O_3 via the well-known[31] cycle:

$$R + O_2 \xrightarrow{M} RO_2 \quad (6)$$

$$RO_2 + NO \rightarrow RO + NO_2 \quad (7)$$

$$NO_2 + h\nu \rightarrow NO + O(^3P) \quad (8)$$

$$O(^3P) + O_2 \xrightarrow{M} O_3 \quad (9)$$

Alternatively, Cl can react with O_3, leading to its destruction in the troposphere. However, the reaction of chlorine atoms with organics is essentially diffusion controlled for all but the smallest ($<C_3$) alkanes, and given the ubiquitous presence of

* Author to whom correspondence should be addressed. Phone (714) 824-7670. E-mail bjfinlay@uci.edu.

[⊗] Abstract published in *Advance ACS Abstracts,* January 1, 1997.

S1089-5639(96)02122-6 CCC: $14.00

organics in the troposphere, reactions 6−9 are the likely path under most tropospheric conditions.

Reaction 1 produces HCl, which does not absorb light in the troposphere. It can be recycled to atomic chlorine, but the reaction is relatively slow. As a result, if reaction 1 predominates over reactions 2−4 in the troposphere, the role of atomic chlorine in the troposphere is not expected to be very important.

The results of recent field studies[3−5] suggest that chlorine atoms do play a role in the oxidation of organics in the marine boundary layer. Although they do not appear to be responsible for a significant loss of organics such as tetrachloroethene on a global scale,[32,33] generation of chlorine atoms in the marine boundary layer at concentrations as high as 10^4-10^5 atoms cm^{-3} has been predicted.[34,35] Atomic chlorine at these concentrations would certainly be expected to impact the chemistry in the marine boundary layer as well as coastal regions, for example by decreasing the amount of organics emitted by the ocean which reach the free troposphere.

Although the kinetics of reactions 1−4 remain somewhat controversial, there is increasing evidence that water adsorbed on defects on the surface plays a key role. For example, the HNO_3 reaction with single crystals of NaCl(100) in an ultra high vacuum (UHV) system, where there is no detectable amount of surface water, is relatively slow, with a reaction probability of $(4 \pm 2) \times 10^{-4}$.[20] On the other hand, the reaction with NaCl powders is much faster,[21,23,25,27] with a reaction probability of $\sim(1-2) \times 10^{-2}$. Recent studies in this laboratory[27] show that water adsorbed on defects on the powders is the controlling factor in these reactions, consistent with the fact that water-free single crystals react much more slowly. While water does not adsorb to the (100) face of single-crystal NaCl at room temperature,[36−38] it does adsorb to surface defects[37,49−52] and is not readily removed by pumping and heating at moderate temperatures (∼400 K).[27]

Furthermore, water appears to play an important role in altering both the chemistry and morphology of preexisting nitrate layers on the crystal surface. For example, in recent studies[29,30] single crystals of NaCl [with either the (100) or (111) faces exposed] were treated with HNO_3 to form a thin surface nitrate layer. When these crystals were subsequently exposed to water vapor at pressures well below the deliquescence point, microcrystallites of $NaNO_3$ were formed and a fresh NaCl surface was regenerated.[29] In addition, some water dissociation occurs, leaving hydroxide ions on the surface.[30]

While significant progress is being made on understanding the interactions of gases with solid NaCl on a molecular level, it is not clear how this will translate to the analogous reactions with the mixture of salts found in sea salt particles which also contain hydrated salts and trace amounts of transition metals. Here we report studies of the reaction of gaseous NO_2 with a mixture of salts representing synthetic sea salt and, for direct comparison, some additional studies of the NO_2−NaCl reaction. We show that hydrated salts play a key role in both the kinetics and mechanism of reaction.

Experimental Section

The DRIFTS apparatus has been described previously in detail.[19] Briefly, the system consists of a Harrick Scientific diffuse reflectance accessory (Model DRA-2CS) surrounded by a vacuum reaction chamber (Model HVC-DR2) located in the sampling compartment of a Mattson RS Fourier transform infrared spectrometer equipped with an MCT detector. Spectra were collected over the range 4000−700 cm^{-1} with a spectral resolution of 1 cm^{-1}. In most cases, an average of 64 scans was used.

Three different salts were used in this study: Instant Ocean, NaCl, and $MgCl_2 \cdot 6H_2O$. Each salt was first placed in a Wig-L-Bug ball mill (Crescent Dental Manufacturing Co.) and ground for 5 min. Weighed amounts (∼250 mg) of sample were then packed into the sample cup (11 mm diameter, 2 mm depth) of the reaction chamber using a packing device similar to that described by TeVrucht and Griffiths.[39] The sample could be heated and the temperature of the sample measured by a thermocouple placed directly underneath. The walls of the reaction chamber were cooled by water flowing through a surrounding jacket. The inside of the reaction chamber was coated with a halocarbon wax (Halocarbon Products, Series 1500) to prevent corrosion of the chamber walls and uptake of gases. The shape and size of the particles were evaluated using scanning electron microscopy (SEM). Images of the salt particles were recorded using a JEOL JSM 6300V scanning electron microscope.

A regulated stream of carrier gas was pumped through the reaction chamber and salt pellet via an outlet at the bottom of the sample holder. NO_2 was added from calibrated storage bulbs into the stream of carrier gas and its concentration calculated from the measured pressure (MKS Baratron pressure gauge with Type 670 readout) decrease in a known volume. The pressure inside the chamber was measured by a capacitance manometer (Edwards Model 600 AB pressure transducer and Model 1570 readout) and was in the range 5−10 Torr. The residence time in the cell was approximately 1 s.

In a typical experiment, the sample was placed into the cup and heated to 400 K for 4−5 h in a stream of dry carrier gas to remove surface-adsorbed water. The water desorption was followed by the decrease in the infrared absorption bands of surface-adsorbed water at ∼3400 and 1635 cm^{-1}. When the intensity of these bands stopped decreasing, the sample was cooled to room temperature and a new background spectrum taken. (It should be noted that, under these conditions, some surface-adsorbed water still remains; as previously demonstrated, treating the salt with D_2O leads to a further decrease in the 3400 cm^{-1} band as the remaining surface water is replaced by D_2O.[19]) The salt was then exposed to measured concentrations of NO_2, and the formation of nitrate followed as a function of time by DRIFTS. The NO_2 concentrations were in the range $(1.4-24.4) \times 10^{14}$ molecules cm^{-3}. All experiments were conducted at room temperature.

For volumetric BET (Brunauer, Emmett, and Teller model) surface area determination,[40] the entire pellet was placed inside a glass tube of small diameter. The sample was heated under vacuum overnight using an infrared lamp to remove adsorbed gases. The surface area was calculated from the measured amount of nitrogen adsorbed on the salt surface at 77 K. The "dead volume" over the salt and between the particles themselves was determined in a similar manner using helium which is not adsorbed at 77 K.

In order to calculate reaction probabilities, the absolute number of nitrate ions formed must be known. To relate the infrared absorption after reaction in the DRIFTS reaction chamber to the absolute number of nitrate ions, the pellets were chemically analyzed for nitrate using a colorimetric method described by Greenberg et al.[41] Each pellet was dissolved in ultrapure water (NANOpure Analytical Deionization System, Type D4700, Barnstead/Thermolyne) followed by reduction of the nitrate to nitrite on an activated Cd column. Highly colored azo dye was developed by diazotization with sulfanilamide and coupling with *N*-(1-naphthyl)ethylenediamine. Absorbance of the dye was measured at 540 nm, with a sensitivity of 2×10^{16} ions per 250 mg pellet. A linear relationship was observed

TABLE 1: Composition of Synthetic Sea Salt

element	wt %	element	wt %
water[a]	13.88	nitrogen	$8 \times 10^{-5}-2 \times 10^{-3}$
chloride	47.53	zinc	$1 \times 10^{-5}-4 \times 10^{-5}$
sodium	26.45	lead	1×10^{-5}
sulfate	6.41	selenium	1×10^{-5}
magnesium	3.19	arsenic	$8 \times 10^{-6}-6 \times 10^{-5}$
calcium	1.00	copper	$3 \times 10^{-6}-2 \times 10^{-4}$
potassium	0.952	tin	8×10^{-6}
bicarbonate	0.356	iron	$5.0 \times 10^{-6}-5.0 \times 10^{-5}$
bromide	0.16	cesium	$\sim 5 \times 10^{-6}$
strontium	0.033	manganese	3×10^{-6}
boron	0.012	phosphorus	$3 \times 10^{-6}-3 \times 10^{-4}$
fluoride	0.0035	thorium	$\leq 1 \times 10^{-6}$
rubidium	5×10^{-4}	mercury	8×10^{-7}
aluminum	$4 \times 10^{-4}-5 \times 10^{-3}$	uranium	$4 \times 10^{-7}-4 \times 10^{-6}$
lithium	3×10^{-4}	cobalt	3×10^{-7}
barium	1×10^{-4}	nickel	$3 \times 10^{-7}-1 \times 10^{-6}$
iodide	1.3×10^{-4}	radium	2×10^{-13}
silicate	$1 \times 10^{-4}-0.02$	titanium	trace

[a] Associated primarily with hydrates (see text).

between the integrated infrared absorption due to nitrate ions and their concentrations measured using the wet chemical technique. The relationship was analyzed as integrated absorbance from 1300−1550 cm^{-1}(ν_3 region) = $S[NO_3^-]$. The constant S was calculated to be $(3.6 \pm 0.6) \times 10^{-18}$ integrated absorbance units per ion for nitrate in the synthetic sea salt and $(2.7 \pm 0.4) \times 10^{-17}$ integrated absorbance units per nitrate ion in the NaCl reaction (errors are $\pm 2\sigma$). The different values of S may be due to several factors. As discussed in detail elsewhere,[19] the absolute calibration of the infrared absorbances using the average pellet nitrate determined by the wet chemical technique is sensitive to the portion of the pellet interrogated by the infrared beam, which depends in part on particle size. In addition, as shown below, hydrates rather than NaCl appear to be the major reacting species in the synthetic sea salt reaction, so that the chemical form and environment of the nitrate may be different in the two cases.

All salts used in this study were prepared by grinding commercially available solids. The synthetic sea salt was "Instant Ocean" (Aquarium Systems, Mentor, OH), the composition of which is given in Table 1. The sodium chloride was from single-crystal cuttings (Harshaw), and the $MgCl_2 \cdot 6H_2O$ (Sigma) was ACS reagent grade. Nitrogen dioxide was prepared by the reaction of nitric oxide (Matheson, CP grade, >99.0%) with excess oxygen (UHP, Union Carbide, ≥99.993%). NO_2 was condensed as white crystals at 195 K and excess oxygen pumped away. Dry gaseous nitric acid was obtained from a 2:1 mixture (by volume) of concentrated sulfuric (Fisher, ACS grade) and nitric acids (Spectrum, ACS grade). Some experiments were carried out using D_2O (99.9%, Cambridge Isotope Laboratory). Helium (UHP, >99.999%, Liquid Carbonic) and air (Ultra-Zero air, Liquid Carbonic, impurities: H_2O <2 ppm, CO <1 ppm, CO_2 <1 ppm, NO <0.1 ppm, total hydrocarbons <0.1 ppm) were used as the carrier gases. In several runs, nitrogen (UHP, >99.999% Liquid Carbonic) was used as a carrier gas to test for diffusion effects.

Results and Discussion

1. Characterization of the Size of the Salt Particles. An SEM image of the ground synthetic sea salt powder used in these experiments is shown in Figure 1. The synthetic sea salt particle size range is approximately 0.1−5 μm, with smaller particles predominating. This is consistent with the measured BET surface area of 2.35×10^4 cm^2 per 250 mg pellet, which one would calculate for monodisperse nonporous cubes with sides of length 0.3 μm.

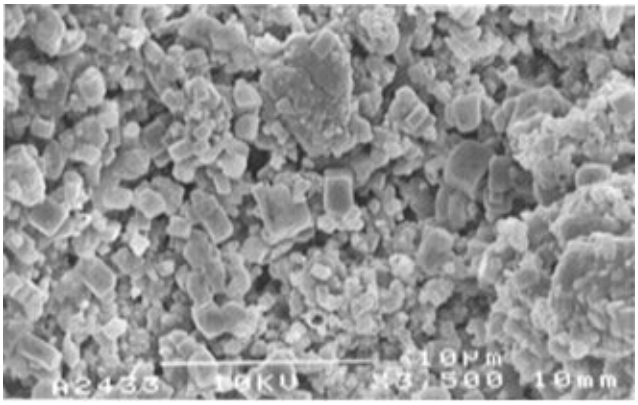

Figure 1. Scanning electron microscope image of a typical ground synthetic sea salt sample. The bar is 10 μm.

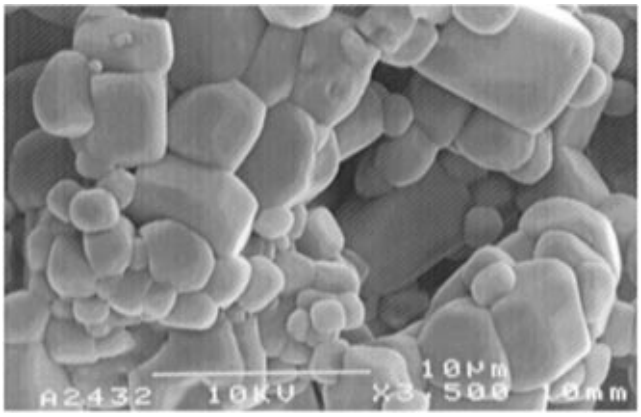

Figure 2. Scanning electron microscope image of a typical ground NaCl sample. The bar is 10 μm.

Figure 2 shows a similar image for the ground NaCl powders which typically have sizes in the range ~1−10 μm. The BET measurements gave a surface area of 2.9×10^3 cm^2 per 250 mg pellet, consistent with monodisperse, nonporous cubes with sides of length 2.4 μm.

2. Reaction of NO_2 with Synthetic Sea Salt. The development of the infrared bands with time was followed during the course of the reaction of synthetic sea salt with NO_2. A typical DRIFTS spectrum from the reaction of NO_2 in air with synthetic sea salt after 2 min reaction time is shown in Figure 3a. Strong infrared absorption bands are observed in the 1300−1550 cm^{-1} region. In addition, there are weaker bands at 1635, 1022, and 815 cm^{-1}, and a broad absorption is at 3370 cm^{-1}.

The bands at 3370 and 1635 cm^{-1} are identified as adsorbed water by comparison to a spectrum of the synthetic sea salt which had been exposed to gaseous water (Figure 3b). The formation of adsorbed water is not observed in similar NaCl experiments (inset to Figure 3a) and is generally much smaller for the synthetic sea salt reaction carried out in He carrier gas. As shown by experiments described below, negative peaks at 3670 and 1610 cm^{-1} are anticipated due to a decrease in the bound water of hydration in the crystalline hydrates in the mixture, which can be released during the reaction.

The free nitrate ion has D_{3h} point group symmetry and four fundamental vibrations: the ν_3 antisymmetric stretch (1390 cm^{-1}), the ν_1 symmetric stretch (1050 cm^{-1}), the ν_2 out-of-plane bend (831 cm^{-1}), and the ν_4 in-plane bend (720 cm^{-1}).[42] By analogy to earlier studies of the NaCl−NO_2 reaction,[19] the infrared bands in the 1300−1550 cm^{-1} region and at 1022 and 815 cm^{-1} are assigned to the ν_3, ν_1, and ν_2 fundamentals of the surface nitrate ions formed during the reaction. The ν_4 band is

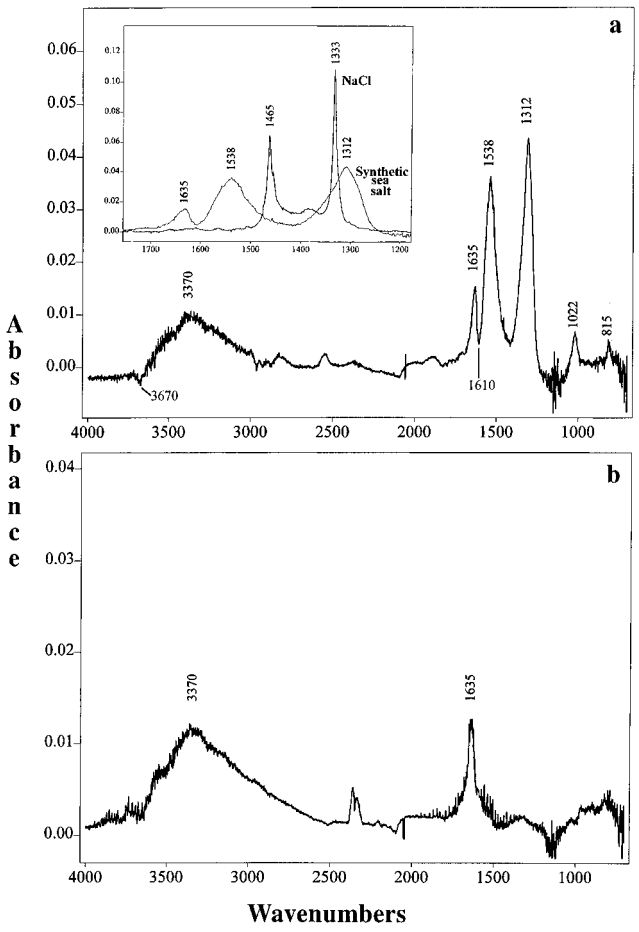

Figure 3. DRIFTS spectrum from (a) the reaction of synthetic sea salt with NO_2 (2.4×10^{15} molecules cm^{-3} for 2 min) in air as the carrier gas at room temperature. The inset compares the spectrum to that from the reaction of NaCl with NO_2 (6.6×10^{14} molecules cm^{-3} for 0.5 min); (b) water adsorbed on synthetic sea salt. Gaseous water ($<5.0 \times 10^{15}$ molecules cm^{-3}) was expanded into the reaction cell and pumped out after several minutes. (The peak at ~2350 cm^{-1} is an increase in CO_2 in the sample compartment as the purge changed.)

too weak to be observed at the low extent of reaction used in these studies.

The ν_3 region shows two absorption bands at 1538 and 1312 cm^{-1}. The positions of these two peaks are the same regardless of whether the reaction is carried out with He or air as the carrier gas. However, they exhibit different time dependencies in the two carrier gases. The peaks were deconvoluted, and the ratio of the peak heights at 1312 and 1538 cm^{-1}, $R_{1312/1538}$, was calculated. When the reaction was carried out in air, the ratio increased from ~0.9 at the beginning of the reaction to a value of 1.3 at longer reaction times, whereas this ratio was approximately constant at $R_{1312/1538} = 1.3$ for experiments carried out in He as a carrier gas. The same behavior was observed without peak deconvolution.

For the NO_2-NaCl reaction, two bands were also observed in this region but at different positions, 1333 and 1465 cm^{-1} (inset to Figure 3a), than those for the synthetic sea salt reaction. Furthermore, the bands are much broader for the reaction of the synthetic sea salt. Since the synthetic sea salt is a mixture of salts, the different band positions and band shapes may be due to reaction of different crystalline components in the mixture. Preliminary X-ray diffraction analysis identified the presence of $MgCl_2 \cdot 6H_2O$, consistent with the composition of the synthetic sea salt provided by the manufacturer (Table 1) and with the composition of recommended mixtures used to mimic sea salt.[43] Other hydrates commonly present[43] in smaller

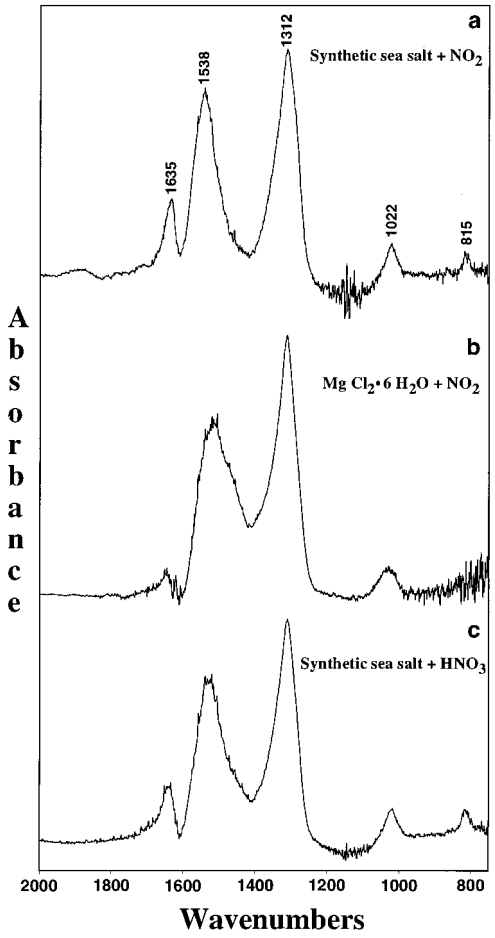

Figure 4. DRIFTS spectra of (a) synthetic sea salt after reaction with NO_2 (2.4×10^{15} molecules cm^{-3} for 2 min), (b) $MgCl_2 \cdot 6H_2O$ with NO_2 (9.1×10^{14} molecules cm^{-3} for 35 min), and (c) synthetic sea salt with gaseous HNO_3 (1.2×10^{14} molecules cm^{-3} for 2 min).

quantities are $CaCl_2 \cdot 2H_2O$ and $SrCl_2 \cdot 6H_2O$. Therefore, to test whether the infrared bands observed in the reaction of synthetic sea salt are associated with hydrates in the mixture, we also studied the reaction of NO_2 with the dominant hydrate species, $MgCl_2 \cdot 6H_2O$.

Figure 4 compares the spectrum from the synthetic sea salt reaction with NO_2 to that from the corresponding $MgCl_2 \cdot 6H_2O$ reaction. For comparison, a spectrum from the reaction of synthetic sea salt with gaseous HNO_3, where nitrate is also the expected product, is shown. The infrared bands in the synthetic sea salt$-NO_2$ reaction are similar to the nitrate bands from the HNO_3 reaction with synthetic sea salt. In addition, they are similar to those from the reaction of NO_2 with $MgCl_2 \cdot 6H_2O$ rather than with NaCl (inset Figure 3a). This confirms that the 1312 and 1538 cm^{-1} bands in the synthetic sea salt reaction with NO_2 are due to surface nitrate. Furthermore, the similarity in the positions of the peaks to those from the $MgCl_2 \cdot 6H_2O$ reaction with NO_2 suggests that the surface nitrate in the reaction of the synthetic sea salt is associated with hydrates in the mixture.

It is important to note that $MgCl_2 \cdot 6H_2O$ is not the only crystalline hydrate present and others such as $CaCl_2 \cdot 2H_2O$ and $SrCl_2 \cdot 6H_2O$ would be expected to react in a similar manner. For the purposes of these initial studies of the mixture, $MgCl_2 \cdot 6H_2O$ was used as a surrogate for all of the hydrates.

The two bands at 1333 and 1465 cm^{-1} formed initially in the NaCl reaction were previously assigned[19] to nitrate ions in different environments on the crystal surface; at longer reaction times a number of overlapping bands also develop. An alternate

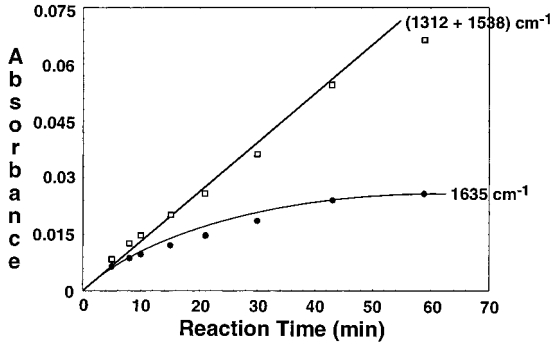

Figure 5. Time dependence of nitrate bands in the ν_3 region and of the surface-adsorbed water band (peak height at 1635 cm^{-1}) in the reaction of NO_2 (2.8×10^{14} molecules cm^{-3}) with synthetic sea salt in air as the carrier gas. The nitrate absorbance is the sum of the peak heights at 1312 and 1538 cm^{-1} obtained by deconvoluting the 1312, 1538, and 1635 cm^{-1} bands.

assignment for the two bands that are initially formed, proposed by Rowland et al.,[44] is that these bands are due to the transverse optical (TO) and longitudinal optical (LO) modes associated with the doubly degenerate ν_3 vibration. This is analogous to the assignment of Peters and Ewing[28] of two bands at 1360 and 1414 cm^{-1} to the splitting of the doubly degenerate ν_3 mode in the NO_2 reaction with the (100) face of NaCl(100) single crystals. The current experiments on synthetic sea salt cannot distinguish between these two interpretations, especially given the large variety of reactive crystals in the mixture, as well as different reactive sites in the form of defects.

The extent of surface coverage of nitrate at the longest reaction time in Figure 5 (59 min) can be estimated from the effective absorption coefficient determined for nitrate ($S = (3.6 \pm 0.6) \times 10^{-18}$ integrated absorbance units per ion), which translates into 2.4×10^{18} nitrate ions at 59 min. Using the BET surface area of 2.35×10^4 cm^2 per pellet and 6.4×10^{14} Cl^- ions per cm^2 of surface area for NaCl as a surrogate,[45] the total number of surface chloride ions in the pellet is 1.5×10^{19}. Thus at the longest reaction times used in our kinetic studies, the nitrate formed corresponds to about 16% of a monolayer. However, it must be emphasized that this assumes that nitrate is evenly distributed over the salt surface, which may not be the case if reactions at surface defects dominate.

Figure 5 shows the time dependence of both the nitrate bands in the ν_3 region and the surface-adsorbed water band at 1635 cm^{-1} during a typical reaction of synthetic sea salt with NO_2 in air. While the nitrate formation continues to increase with reaction time, the water band increases initially, followed by a slower rate of formation at longer reaction times. This nonlinear increase in surface-adsorbed water may be due to its simultaneous removal by the carrier gas which is pumped through the salt during the course of the reaction. The rate of such removal would be expected to increase with reaction time once available surface sorption sites become completely occupied.

There are at least two potential sources of water: that which is bound in the crystal structure of the stable hydrates and that which is trapped in occlusions between the crystals. Since the infrared spectra indicate that the hydrates are clearly one of the reacting species, the reaction of NO_2 with hydrates may disrupt the crystal lattice and release the bound water of hydration. Crystal structures determined by neutron diffraction of $MgCl_2 \cdot 6H_2O$,[46] $CaCl_2 \cdot 6H_2O$,[47] and $SrCl_2 \cdot 6H_2O$[47] and by X-ray diffraction of $CaCl_2 \cdot 2H_2O$[48] on single crystals show one common feature: each cation is surrounded by H_2O in a characteristic coordination for each compound, with water molecules hydrogen bonded to the chloride ions and oxygen coordinated to the metal

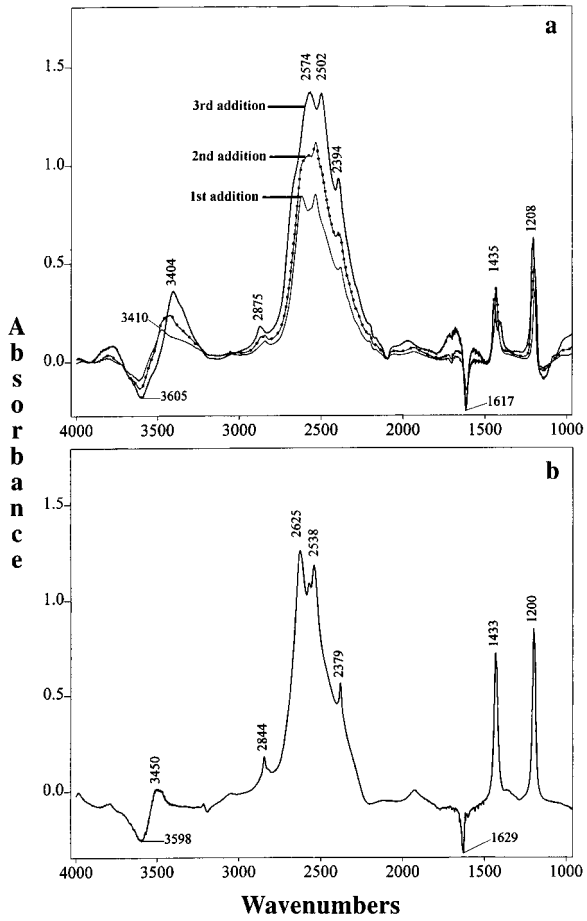

Figure 6. DRIFTS spectra of (a) synthetic sea salt after sequential exposure to D_2O (2.0×10^{17} molecules cm^{-3} for 10 min) followed by pumping and (b) $MgCl_2 \cdot 6H_2O$ exposed to D_2O (2.0×10^{17} molecules cm^{-3} for ~10 min).

ions. Removal of the chloride ion in the form of gaseous ClNO disrupts this crystal structure, freeing the water of hydration. Alternatively, or in addition, reaction with NO_2 may disrupt crystals which are clustered together, freeing water trapped between them.

To test whether the bound water of hydration could be one source of the surface-adsorbed water, several experiments were carried out to replace the bound water of hydration in the hydrates in the synthetic sea salt with D_2O. Synthetic sea salt was first dried by heating and pumping as described above and was then exposed to gaseous D_2O at a concentration of 2.0×10^{17} molecules cm^{-3} for 10 min, followed by pumping. This was repeated three times. As seen in Figure 6a, bands at 3400−3410, 2400−2600, 1500−1700, 1435, and 1208 cm^{-1} increased while bands at 3605 and 1617 cm^{-1} decreased simultaneously.

Adsorption of water molecules on alkali halide surfaces has been extensively studied[49−52] using infrared spectroscopy. On the basis of the literature[49−52] and the experiment shown in Figure 3b, the broad bands at 3400−3410 cm^{-1} and in the 1500−1700 cm^{-1} region which increase are assigned to surface-physisorbed H_2O. Smart and Sheppard[51] also studied D_2O adsorption on NaCl and reported bands at 2735, 2570, 2520, and 1190 cm^{-1}. The bands in the 2500−2700 cm^{-1} region were assigned to hydrogen-bonded OD stretching vibrations and those at 1190 cm^{-1} to bending vibrations of adsorbed D_2O.[51] Thus, the bands at 2400−2600 and 1208 cm^{-1} in Figure 6a can be attributed to adsorbed D_2O.[51] The band at 1435 cm^{-1} originates from adsorbed HDO[42] formed by isotope exchange between H_2O associated with the salt and the added D_2O.

As seen in Figure 6a, the increase in the infrared bands assigned to surface-adsorbed H_2O, D_2O, and HDO is accompanied by a decrease in bands at 3605 and 1617 cm^{-1}. Since D_2O should replace water in the salt, these bands are assigned to bound water of hydration and decrease as the exchange occurs.

To confirm this, a similar D_2O replacement experiment was carried out with $MgCl_2 \cdot 6H_2O$, the major hydrate present in synthetic sea salt. As seen in Figure 6b, upon exposure of the hydrate to D_2O, bands at 3598 and 1629 cm^{-1} decrease, while those due to surface-adsorbed H_2O, D_2O, and HDO increase. In short, water of hydration both in $MgCl_2 \cdot 6H_2O$ and in the synthetic sea salt mixture can be replaced by D_2O. This replacement displaces the water from the crystal lattice onto the salt surface where it can be detected as surface-adsorbed water.

As seen in Figure 3a, the NO_2 reaction with synthetic sea salt, which results in an increase in the infrared bands assigned to surface-adsorbed water, is also accompanied by a small negative peak at 3670 cm^{-1} (and perhaps also at 1610 cm^{-1}), both of which are partially obscured by the simultaneous increase in bands due to nitrate and surface-adsorbed water. Although they are not at exactly the same positions as the negative peaks observed in the D_2O replacement experiments, these negative peaks are most reasonably assigned to bound water of hydration which is released during the reaction and becomes physisorbed surface water. The increase in the area of the broad 3400 cm^{-1} band is larger than the decrease in the 3670 cm^{-1} peak, although the true decrease in the latter may be partially obscured by the band overlap. This suggests that part of the increase in surface-adsorbed water may also be due to release of water trapped between crystal clusters.

3. Kinetics and Mechanisms. The most general kinetic equation for the formation of nitrate in this reaction is given by the following rate law

$$\text{rate } (R) = \mathrm{d}\{NO_3^-\}/\mathrm{d}t = k\{X^-\}^m[NO_2]^n \qquad \text{(I)}$$

where $\{NO_3^-\}$ and $\{X^-\}$ are surface concentrations of nitrate and halogen anions (chloride or bromide) in ions cm^{-2} (please note the braces are used to distinguish surface concentrations from gas phase concentrations), k is an effective rate constant, $[NO_2]$ is gas phase concentration in molecules cm^{-3}, and m and n are the reaction orders with respect to X^- and NO_2, respectively. A plot of ln R against ln $[NO_2]$ should be linear with a slope equal to the reaction order with respect to $[NO_2]$, n, at smaller surface conversions where $\{X^-\}$ is constant.

DRIFTS can be used to study kinetics since the formation of nitrate can be followed during the reaction. However, as discussed in detail elsewhere,[19] there are substantial uncertainties in this application of DRIFTS which lead to larger uncertainties than those given by the statistical errors. For example, the measured absorbance is sensitive to particle size as well as to reproducible packing of the sampling cup.[39,53,54] Differences in particle size due to differences in grinding times and procedures may also affect the number of surface defects and hence potential reactive sites. In addition, the formation of nitrate does not occur evenly throughout the pellet; a trend of decreasing nitrate with increasing depth in the pellet has been observed in the reaction of NO_2 with NaCl.[19] Finally, infrared absorbances must be calibrated using wet chemical measurements of the average nitrate in the total pellet; as discussed above, this calibration is sensitive to the portion of the pellet interrogated by the infrared beam. These potential systematic errors lead to overall uncertainties in the reaction probabilities (see below) that are much larger than the statistical errors, as illustrated below for the NaCl reaction with NO_2. However, the error introduced into the determination of the reaction order is smaller since absolute calibration of the absorbance is not required, and other systematic errors are in the same direction for all experiments.

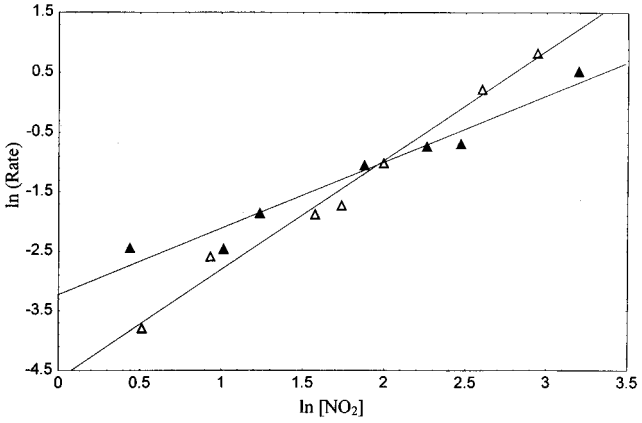

Figure 7. ln−ln plot of the rate of NO_3^- formation as a function of NO_2 concentration for the reaction of synthetic sea salt with NO_2 in helium (open triangles) and air (filled triangles). The rate of nitrate formation is in units of integrated absorbance min^{-1}, and the NO_2 concentration is in units of 10^{14} molecules cm^{-3}. Statistical errors (2σ) are typically about the size of the points. See text for discussion of systematic errors.

In these studies, the NO_2 concentration is constant because a continuous flow was used. In the earliest stages of the reaction, the number of surface X^- ions is large compared to that of the nitrate ions formed so that this concentration is approximately constant. Under these conditions, eq I can be integrated to eq II:

$$\{NO_3^-\} = k\{X^-\}^m[NO_2]^n t \qquad \text{(II)}$$

A plot of the surface nitrate concentration, or alternatively the total integrated absorbance in the ν_3 region, versus reaction time is thus expected to be linear for small extents of reaction at the surface. The integrated absorbances can be converted to the absolute number of nitrate ions using the wet chemical analysis for nitrate as discussed above.

In the reaction of both the synthetic sea salt and NaCl, the amount of nitrate formed increased linearly at the beginning of the reaction (Figure 5). At longer reaction times (not shown in Figure 5), the increase leveled off as the surface became saturated with nitrate ions. The initial linear portion of plots of integrated absorbance versus reaction time was used to determine the rate of nitrate formation, R, when the assumption of constant $\{X^-\}$ is valid.

Figure 7 shows a ln−ln plot for the reaction of synthetic sea salt with NO_2 using either helium or air as a carrier gas. For experiments in helium, the slope of the line, i.e. the reaction order n, is $n = 1.8 \pm 0.2$ (2σ), while experiments performed in air have a slope $n = 1.2 \pm 0.2$ (2σ).

Diffusion effects on the kinetics of the NO_2 reaction with NaCl were observed by Peters and Ewing[28] in a static system using single crystals of NaCl and higher NO_2 concentrations. Although their conditions are quite different than those in the present DRIFTS flow system, several experiments were carried out during the present studies on the reaction of NO_2 with synthetic sea salt in N_2 compared to that in He as the carrier gas to test for effects of diffusion. The measured rates of formation of the ν_3 band (in integrated absorbance units min^{-1}) were 0.20 in N_2 and 0.14 in He at NO_2 concentrations of (2.1−2.2) × 10^{14} molecules cm^{-3}. At an NO_2 concentration of 6.1

TABLE 2: Kinetics of the NaCl + NO_2/N_2O_4 Reaction in Helium and in Air

expt no.	$[NO_2]$ (10^{14} molec cm^{-3})	$[N_2O_4]^a$ (10^{10} molec cm^{-3})	rate^b (int absorb. min^{-1})	$R_{NO_3^-}{}^c$ (10^{13} ions s^{-1})	C^d (10^{17} collisions s^{-1})	Φ^e (10^{-4})
			In Helium			
1	4.0	4.1	0.408	25.0	7.90	3.1
2	3.4	2.8	0.376	23.1	5.52	4.2
3	5.9	8.7	1.08	66.1	16.9	3.9
4	2.4	1.4	0.151	9.30	2.74	3.4
5	1.4	0.49	0.0812	4.99	0.953	5.2
					$\Phi_{av} = (4.0 \pm 1.6) \times 10^{-4}$ (2σ)	
			In Air			
6	4.1	4.3	0.219	13.4	8.29	1.6
7	6.6	11.0	1.05	64.6	21.1	3.1
8	23.7	140	6.35	390	274	1.4
9	1.5	0.57	0.0833	5.11	1.10	4.6
10	1.7	0.73	0.0980	6.02	1.41	4.3
					$\Phi_{av} = (3.0 \pm 2.9) \times 10^{-4}$ (2σ)	

[a] Calculated from the equilibrium constant $K_{10} = 2.5 \times 10^{-19}$ cm^3 molecule^{-1}. [b] Observed rate of nitrate formation obtained from the integrated absorbance in the ν_3 region. [c] Absolute rate of nitrate formation obtained by calibrating the infrared absorbance using a wet chemical technique described in the text. [d] Collision rate of N_2O_4 with the NaCl surface ($A = 2.9 \times 10^3$ cm^2 per pellet). [e] Reaction probability for the gaseous N_2O_4 with the solid NaCl surface reaction.

TABLE 3: Kinetics of the Reaction of NO_2/N_2O_4 in Helium with Synthetic Sea Salt

expt no.	$[NO_2]$ (10^{14} molec cm^{-3})	$[N_2O_4]^a$ (10^{10} molec cm^{-3})	rate^b (int absorb. min^{-1})	$R_{NO_3^-}{}^c$ (10^{13} ions s^{-1})	C^d (10^{17} collisions s^{-1})	Φ^e (10^{-4})
1	7.4	14	0.363	167	207	0.81
2	13.5	46	1.25	576	692	0.83
3	19.0	90	2.30	1060	1370	0.77
4	4.8	5.8	0.154	70.8	88.8	0.80
5	1.7	0.70	0.0231	10.5	10.6	0.99
6	2.5	1.6	0.0764	34.8	24.5	1.4
7	5.7	8.1	0.179	82.4	123	0.67
					$\Phi_{av} = (0.9 \pm 0.5) \times 10^{-4}$ (2σ)	

[a] Calculated from the equilibrium constant $K_{10} = 2.5 \times 10^{-19}$ cm^3 molecule^{-1}. [b] Observed rate of nitrate formation obtained from the integrated absorbance in the ν_3 region. [c] Absolute rate of nitrate formation obtained by calibrating the rate of infrared absorbance using a wet chemical technique as described in the text. [d] Collision rate of N_2O_4 with the synthetic sea salt surface ($A = 2.35 \times 10^4$ cm^2 per pellet). [e] Reaction probability for the gaseous N_2O_4 with the solid synthetic sea salt surface reaction.

TABLE 4: Kinetics of the Reaction of NO_2 in Air with Synthetic Sea Salt

expt no.	$[NO_2]$ (10^{14} molec cm^{-3})	rate^a (int absorb. min^{-1})	$R_{NO_3^-}{}^b$ (10^{13} ions s^{-1})	C^c (10^{22} collisions s^{-1})	Φ^d (10^{-8})
1	24.4	1.60	751	52.6	1.4
2	11.8	0.515	240	25.5	0.94
3	9.6	0.503	235	20.7	1.1
4	3.4	0.145	67.6	7.41	0.91
5	6.5	0.357	167	14.1	1.2
6	2.8	0.0785	36.6	5.93	0.62
7	1.6	0.0799	37.3	3.39	1.1
				$\Phi_{av} = (1.0 \pm 0.5) \times 10^{-8}$ (2σ)	

[a] Observed rate of nitrate formation obtained from the integrated absorbance in the ν_3 region. [b] Rate of nitrate formation from calibration of the integrated absorbance with the wet chemical technique. [c] Collision rate of NO_2 with the synthetic sea salt surface ($A = 2.35 \times 10^4$ cm^2 per pellet). [d] Reaction probability for the gaseous NO_2 reaction with synthetic sea salt.

$\times 10^{14}$ molecules cm^{-3}, the rate was 0.38 in He; in N_2 at NO_2 concentrations of 3.0 and 7.1 $\times 10^{14}$ molecules cm^{-3} which bracket the He run, the rates were 0.23 and 1.1, respectively. (The absolute values of these rates should not be compared directly to those in Tables 2−4 since they were not calibrated using the wet chemical technique and there may also be differences in particle size, etc.) Within the scatter of these limited number of runs, there is no evidence of diffusion effects which would be expected to give higher rates of nitrate formation in He than in N_2.

In prior studies of the NO_2 reaction with NaCl in this laboratory,[19] the reaction order in NO_2 was found to be $n = 1.6 \pm 0.2$ (2σ; statistical error only) in either air or He. When possible systematic errors are taken into account, we estimated that the reaction order n was within experimental error of 2. For direct comparison to the synthetic sea salt studies, some additional NaCl experiments were carried out. Figure 8 shows a reaction order for NO_2 in helium of 1.8 ± 0.3 (2σ) and in air of 1.6 ± 0.3 (2σ), in agreement with the earlier work.[19] This is consistent with more recent studies of NO_2 at higher concentrations ($(0.37-8.4) \times 10^{16}$ molecules cm^{-3}) with the (100) face of NaCl where the reaction was found to be second order in NO_2.[28]

In short, the linear increase in the nitrate absorbance with time and the linear plots of ln rate versus ln $[NO_2]$ at small extents of reaction show that NO_2 reacts with both NaCl and with synthetic sea salt in a manner consistent with eqs I and II. The reaction is approximately second order in NO_2 for NaCl in both He and air as well as for the reaction of synthetic sea salt in He. The lower reaction order for the synthetic sea salt−NO_2 reaction in air suggests that in the latter case there may be some contribution from a lower order process.

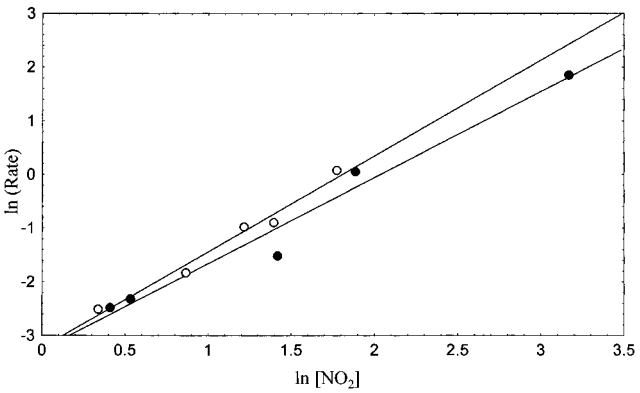

Figure 8. ln−ln plot of the rate of NO_3^- formation as a function of the NO_2 concentration for the reaction of NaCl with NO_2 in helium (open circles) and air (filled circles). The rate of nitrate formation is in units of integrated absorbance min^{-1}, and the NO_2 concentration is in units of 10^{14} molecules cm^{-3}. Statistical errors (2σ) are typically about the size of the points. See text for discussion of systematic errors.

As discussed earlier,[19] a reaction which is second order in NO_2 is consistent with the dimer of NO_2, i.e. N_2O_4, being the reactive species. In this case, the reaction mechanism involves first the formation of the dimer

$$2NO_2 \leftrightarrow N_2O_4 \tag{10}$$

followed by reaction of the dimer with the salt

$$N_2O_4 + NaCl \rightarrow ClNO + NaNO_3 \tag{11}$$

The rate law may then be expressed as

$$d\{NO_3^-\}/dt = k_{11}\{X^-\}^m[N_2O_4] = k_{11}K_{10}\{X^-\}^m[NO_2]^2 \tag{III}$$

where K_{10} is the equilibrium constant for the formation reaction (10) of the dimer. The N_2O_4 concentration can be calculated from the measured NO_2 concentration and the well-known equilibrium constant,[55] $K_{10} = 2.5 \times 10^{-19}$ cm^3 $molecule^{-1}$ at 298 K.

The kinetics for gas−solid heterogeneous reactions are normally described in terms of the reaction probability, Φ, which is defined as the ratio of reactive gas−solid collisions to the total number of gas collisions with the surface. The total number of collisions per second can be calculated[31] from the gas kinetic expression $C = A[G](RT/2\pi M)^{1/2}$ where A is the surface area of the salt, [G] is the concentration of N_2O_4, and M is its molecular weight. The reaction probability can then be calculated from the experimentally determined rate of the nitrate formation (in ions/s) compared to the total number of collisions/s:

$$\Phi = R/C \tag{IV}$$

Tables 2 and 3 summarize the results of the experiments for NaCl in air and He and for synthetic salt in He, respectively. In these experiments, the infrared absorbances were calibrated using the wet chemical technique described above in order to obtain reaction probabilities. The reaction probabilities are calculated to be $(4.0 \pm 1.6) \times 10^{-4}$ (2σ) for the N_2O_4−NaCl reaction in He and $(3.0 \pm 2.9) \times 10^{-4}$ (2σ) in air. These can be compared to that reported in our earlier studies,[19] $(1.3 \pm 1.2) \times 10^{-4}$ (2σ). The average particle size in our earlier studies[19] based on the BET measurements was 4 μm, somewhat larger than the 2.4 μm measured here. Hence there may be differences in the number of surface defects, steps, and edges which can influence the reactivity.

There may also be a difference in the amount of surface adsorbed water, which appears to play a role in the kinetics. For example, Peters and Ewing[28] have studied the reaction of NO_2 with the (100) face of NaCl and also find that this reaction is second order. They report a reaction probability for N_2O_4 of $\sim 1 \times 10^{-6}$ for dry NaCl but $\sim 1 \times 10^{-4}$ for NaCl in the presence of water vapor at a concentration of 9.5 mbar. This observation on the effect of water on the kinetics is consistent with the observation that strongly bound water adsorbed to the surface of NaCl powders plays a critical role in its chemistry. For example, Knudsen cell experiments[27] in this laboratory have shown that the reaction of HNO_3 is controlled by surface-adsorbed water. Hence the discrepancies in the reported reaction probabilities for the N_2O_4 reaction with NaCl may also reflect differences in the amount of surface-adsorbed water. In addition, the finely ground powder used here and in the earlier studies[19] undoubtedly have much larger numbers of surface defects compared to the (100) face of single crystals, and these would be expected to react more rapidly, even in the absence of adsorbed water.

These differences of about a factor of 3 for the reaction probability for the NaCl reaction illustrate the uncertainties in the applications of DRIFTS to kinetic measurements discussed earlier. However, such studies do provide at least an order of magnitude estimate of the reaction probabilities for powders that may be more representative of airborne sea salt particles in the marine boundary layer than reactions of relatively defect-free single crystals. In addition, comparison of the kinetics of reaction of such powders with those of single crystals provides insights into the mechanism and the factors which control the reactivity on a molecular level, as illustrated by recent studies of HNO_3 with NaCl.[20,21,23,25,27]

Table 3 shows the results of the synthetic sea salt−NO_2 experiments using He as a carrier gas where the reaction order was observed to be 1.8 ± 0.2 (2σ). Again assuming that N_2O_4 is the reactive species, a reaction probability of $(0.9 \pm 0.5) \times 10^{-4}$ (2σ) is obtained. Although this is slightly lower than the reaction probability for the NaCl−N_2O_4 reaction, one cannot readily distinguish between the two, given that the measured values for the reaction of NaCl powders using DRIFTS are in the range $(1.3-4.0) \times 10^{-4}$. If indeed the reaction probability for synthetic sea salt is smaller than that for NaCl, it may be related to differences in the number of surface defects. The SEM of the ground NaCl (Figure 2) shows quite rounded features rather than the sharp, cubic structure of freshly grown crystals.[29] The concentration of surface defects on these crystals may be larger than for the synthetic sea salt, which would be expected to increase its reactivity. The reaction probabilities in Tables 2 and 3 are quite scattered but tend to show a decreasing trend with increasing NO_2/N_2O_4 concentration. This may be due to a breakdown in the assumption that the concentration of available surface halide ions remains constant at the higher gas concentrations where the reaction is much faster.

In short, the present results show that the reaction probabilities for the reactions of N_2O_4 with NaCl in air or He as well as with synthetic sea salt in He are all about 10^{-4}.

The order of the reaction of synthetic sea salt with NO_2 in air is smaller than that in He, approaching unity. Although the mechanistic source of this decrease is not clear (see below), the reaction probability in this case is calculated assuming first-order kinetics using NO_2 rather than N_2O_4 as the reactant. As seen in Table 4, the reaction probability is calculated to be Φ

$= (1.0 \pm 0.5) \times 10^{-8}$ (2σ). This can be compared to the results of Sverdrup and Kuhlman[56] where reaction probabilities, based on the loss of NO_2 on an artificial sea salt surface, were measured to be in the range $10^{-7}-10^{-6}$ over a range of relative humidities of 44−88%. This is not surprising, given the higher water concentrations used in their studies. It should be noted that if the predominant reacting species in the synthetic sea salt are the hydrates, the reaction probability for the NO_2 reaction with the hydrates must be about 1 order of magnitude faster since the hydrates typically comprise about 12 mol % of the salt mixture.[43]

Because the generation of surface-adsorbed water, H_2O_{ads}, is observed in the reaction of synthetic sea salt in air, it is possible that during the course of the reaction, the uptake of NO_2 into surface-adsorbed water may become important, as observed recently for the uptake of HNO_3 by NaCl.[27] For example, the reaction of NO_2 with surface-adsorbed water is well-known[57−62]

$$2NO_2 + H_2O_{ads} \rightarrow HONO + HNO_3 \qquad (12)$$

and has been shown to be first order in NO_2. The nitric acid formed will react with the synthetic sea salt, which would also form infrared active surface nitrate as well as gaseous HCl. We are not able to observe gaseous products in the DRIFTS experiment. However, the production of HONO and HCl was investigated in a separate experiment by reacting the synthetic sea salt with NO_2 in air under conditions similar to those used in the DRIFTS experiments. The mixture of gaseous products and unreacted NO_2 was expanded into a long path cell (25.6 m) located in the sampling compartment of an FTIR. ClNO was observed as a product as expected, but HONO and HCl were not. While the experimental system was somewhat different, this suggests that reaction 12 followed by the reaction of HNO_3 with the salt is not contributing significantly to the reaction of NO_2 with synthetic sea salt in our studies.

An alternate mechanism involves the formation of an intermediate, **A**, in the hydrate reaction which then reacts with either NO_2 or O_2, e.g.

$$Cl^- \text{ (e.g. in } MgCl_2 \cdot 6H_2O) + NO_2 \leftrightarrow \mathbf{A} \qquad (13, -13)$$

$$\mathbf{A} + NO_2 \rightarrow NO_3^- + ClNO \qquad (14)$$

$$\mathbf{A} + O_2 \rightarrow \mathbf{B} \qquad (15)$$

$$\mathbf{B} + NO_2 \rightarrow \rightarrow \rightarrow ClNO + NO_3^- + O_2 \qquad (16)$$

In the absence of O_2, the mechanism consists of reactions 13 and 14, and if the back-reaction −13 is fast compared to reaction 14, the overall reaction is second order in NO_2. However, if in the presence of O_2 reactions 15 and 16 are fast relative to reaction −13, the reaction will be first order in NO_2.

There is some evidence for the formation of unstable intermediates in the NaCl reaction. An intermediate, tentatively identified as a radical anion intermediate of the type $[Cl\cdots NO_2^-]$,[63] has been observed recently by electron paramagnetic resonance (EPR) in the reaction of NaCl with NO_2. A similar intermediate was observed in the NaBr−NO_2 reaction.[63] As discussed in detail elsewhere,[19,63] reactions 13 and 14 would also give second-order kinetics in NO_2, so that this mechanism cannot be distinguished from reaction with N_2O_4. However, the reaction probabilities in Tables 2 and 3 were calculated on the basis of N_2O_4 being the reactant, since insufficient kinetic and thermodynamic information is available for reactions 13 and 14 to be able to carry out such calculations using this mechanism.

The nature of a possible second intermediate, **B**, is not known but could be similar to a peroxynitrate, e.g. $[Cl\cdots OONO_2]^-$. An analogous intermediate, the peroxonitrite ion ($OONO^-$), has been shown to be an important intermediate in the photolysis of KNO_3.[64] However, if this is the case, it is surprising that the same mechanism does not hold for the NaCl reaction. It is possible that Mg^{2+} present in the synthetic sea salt stabilizes the intermediate, while Na^+ does not. For example, chelation of the intermediate to the metal ion can be envisioned

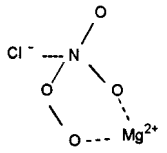

In this case, the coordination between the oxygen in two of the six waters of hydration surrounding the Mg^{2+} must be broken. This, combined with the disruption to the hydrogen bonds to the Cl^- caused by the reaction, would release water of hydration, consistent with our experimental observations.

4. Atmospheric Implications. These studies suggest that hydrates in sea salts, although minor components, play a major role in the chemistry of sea salt particles. As a result, NaCl may not be an adequate model for such reactions. For example, these studies suggest that the order of the reaction of NO_2 with synthetic sea salt in air approaches 1, rather than being approximately second order as is the case for the NaCl reaction, indicating a change in reaction mechanism.

The reaction of synthetic sea salt with NO_2 in the presence of air produces significant amounts of surface-physisorbed water. Given the results of recent studies[27−30] which demonstrate the importance of water in the chemistry of NaCl, the role of the hydrates in providing surface-adsorbed water during the reaction of sea salt particles may be important, particularly in laboratory studies of these reactions.

The reaction of NO_2 with synthetic sea salt is sufficiently slow that it is unlikely to be important in marine areas. However, the differences in kinetics and mechanisms from the corresponding reactions of NaCl indicate that the kinetics and mechanisms of other potential reactants such as $ClONO_2$, N_2O_5, and HNO_3 with synthetic sea salt also need to be investigated in order to properly assess their contribution to tropospheric chemistry.

Conclusions

In summary, the reaction of NO_2 with synthetic sea salt in air is consistent with crystalline hydrates being major contributors to the reaction. The reaction order in NO_2 in air is lower than that for the NaCl reaction and leads to the generation of surface-adsorbed water. A possible explanation is that O_2 reacts with a radical anion intermediate similar to that observed in the NO_2−NaCl reaction.[63] EPR experiments are planned to further explore possible intermediates in these reactions. In addition, the kinetics and mechanisms of reaction of NO_2 and HNO_3 with hydrates found in sea salt are being explored in detail. Finally, studies of HNO_3, N_2O_5, and $ClONO_2$ with synthetic sea salt are underway.

Acknowledgment. We gratefully acknowledge the financial support of the National Science Foundation (Grant No. ATM-9302475), the Department of Energy (Grant No. DE-FG03-94ER61899), and the Swedish OK Environmental Protection

Board (OKs Miljöstiftelse). We thank Dr. George Ewing for helpful comments on the manuscript. We also thank Ms. Dinh Quach for assistance with some of the experiments and Drs. Paul Devlin, Vratislav Langer, James N. Pitts, Jr., John C. Hemminger, Frank Feher, and Jeff Gaffney for helpful discussions.

References and Notes

(1) Finlayson-Pitts, B. J. *Res. Chem. Intermed.* **1993**, *19*, 235.
(2) Graedel, T. E.; Keene, W. C. *Global Biogeochem. Cycles* **1995**, *9*, 47.
(3) Jobson, B. T.; Niki, H.; Yokouchi, Y.; Bottenheim, J.; Hopper, F.; Leaitch, R. *J. Geophys. Res.* **1994**, *99*, 25355.
(4) Singh, H. B.; Gregory, G. L.; Anderson, B.; Browell, E.; Sachse, G. W.; Davis, D. D.; Crawford, J.; Bradshaw, J. D.; Talbot, R.; Blake, D. R.; Thornton, D.; Newell, R.; Merrill, J. *J. Geophys. Res.* **1996**, *101*, 1907.
(5) Wingenter, O. W.; Kubo, M. K.; Blake, N. J.; Smith, T. W., Jr.; Blake, D. R.; Rowland, F. S. *J. Geophys. Res.* **1996**, *101*, 4331.
(6) Blanchard, D. C. *J. Geophys. Res.* **1985**, *90*, 961.
(7) Robbins, R. C.; Cadle, R. D.; Eckhardt, D. L. *J. Meteorol.* **1959**, *16*, 53.
(8) Cadle, R. D.; Robbins, R. C. *Discuss. Faraday Soc.* **1960**, *30*, 155.
(9) Schroeder, W. H.; Urone, P. *Environ. Sci. Technol.* **1974**, *8*, 756.
(10) Chung, T. T.; Dash, J.; O'Brien, R. J. *9th Int. Congr. Electron Microsc.* **1978**, 440.
(11) Finlayson-Pitts, B. J. *Nature* **1983**, *306*, 676.
(12) Finlayson-Pitts, B. J.; Ezell, M. J.; Pitts, J. N., Jr. *Nature* **1989**, *337*, 241.
(13) Livingston, F. E.; Finlayson-Pitts, B. J. *Geophys. Res. Lett.* **1991**, *18*, 17.
(14) Winkler, T.; Goschnick, J.; Ache, H. J. *J. Aerosol. Sci.* **1991**, *22*, S605.
(15) Junkermann, W.; Ibusuki, T. *Atmos. Environ.* **1992**, *26A*, 3099.
(16) Zetzsch, C.; Behnke, W. *Ber. Bunsen-Ges. Phys. Chem.* **1992**, *96*, 488.
(17) Behnke, W.; Scheer, V.; Zetzsch, C. *J. Aerosol. Sci.* **1993**, *24*, S115.
(18) George, C.; Ponche, J. L.; Mirabel, P.; Behnke, W.; Scheer, V.; Zetzsch, C. *J. Phys. Chem.* **1994**, *98*, 8780.
(19) Vogt, R.; Finlayson-Pitts, B. J. *J. Phys. Chem.* **1994**, *98*, 3747; **1995**, *99*, 13052.
(20) Laux, J. M.; Hemminger, J. C.; Finlayson-Pitts, B. J. *Geophys. Res. Lett.* **1994**, *21*, 1623.
(21) Fenter, F. F.; Caloz, F.; Rossi, M. J. *J. Phys. Chem.* **1994**, *98*, 9801.
(22) Timonen, R. S.; Chu, L. T.; Leu, M.-T.; Keyser, L. F. *J. Phys. Chem.* **1994**, *98*, 9509.
(23) Leu, M.-T.; Timonen, R. S.; Keyser, L. F.; Yung, Y. L. *J. Phys. Chem.* **1995**, *99*, 13203.
(24) Karlsson, R.; Ljungström, E. *J. Aerosol Sci.* **1995**, *26*, 39.
(25) Fenter, F. F.; Caloz, F.; Rossi, M. J. *J. Phys. Chem.* **1996**, *100*, 1008.
(26) Caloz, F.; Fenter, F. F.; Rossi, M. J. *J. Phys. Chem.* **1996**, *100*, 7494.
(27) Beichert, P.; Finlayson-Pitts, B. J. *J. Phys. Chem.* **1996**, *100*, 15218.
(28) Peters, S. J.; Ewing, G. E. *J. Phys. Chem.* **1996**, *100*, 14093.
(29) Allen, H. C.; Laux, J. M.; Vogt, R.; Finlayson-Pitts, B. J.; Hemminger, J. C. *J. Phys. Chem.* **1996**, *100*, 6371.
(30) Laux, J. M.; Fister, T. F.; Finlayson-Pitts, B. J.; Hemminger, J. C. X-ray Photoelectron Spectroscopy Studies of the Effects of Water Vapor on Ultra-Thin Nitrate Layers on NaCl. *J. Phys. Chem.*, in press.
(31) Finlayson-Pitts, B. J.; Pitts, J. N., Jr. *Atmospheric Chemistry: Fundamentals and Experimental Techniques*; Wiley: New York, 1986.
(32) Singh, H. B.; Thakur, A. N.; Chen, Y. E.; Kanakidou, M. *Geophys. Res. Lett.* **1996**, *23*, 1529.
(33) Rudolph, J.; Koppmann, R.; Plass-Dülmer, C. *Atmos. Environ.* **1996**, *30*, 1887.
(34) Keene, W. C.; Maben, J. R.; Pszenny, A. A. P.; Galloway, J. N. *Environ. Sci. Technol.* **1993**, *27*, 866.
(35) Pszenny, A. A. P.; Keene, W. C.; Jacob, D. J.; Fan, S.; Maben, J. R.; Zetwo, M. P.; Springer-Young, M.; Galloway, J. N. *Geophys. Res. Lett.* **1993**, *20*, 699.
(36) Estel, J.; Hoinkes, H.; Kaarmann, H.; Nahr, H.; Wilsch, H. *Surf. Sci.* **1976**, *54*, 393.
(37) Fölsch, S.; Henzler, M. *Surf. Sci.* **1991**, *247*, 269.
(38) Fölsch, S.; Stock, A.; Henzler, M. *Surf. Sci.* **1992**, *264*, 65.
(39) TeVrucht, M. L. E.; Griffiths, P. R. *Appl. Spectrosc.* **1989**, *43*, 1492.
(40) Shoemaker, D. P.; Garland, C. W. *Experiments in Physical Chemistry*; McGraw-Hill: New York, 1967.
(41) Greenberg, A. F., Trussell, R. R., Clesceri, L. S., Franson, M. A. H., Eds. *Standard Methods for the Examination of Water and Waste Water*; American Public Health Association, American Water Works Association, and Water Pollution Control Federation; American Public Health Association: Washington, DC, 1985.
(42) Herzberg, G. *Molecular Spectra and Molecular Structure II. Infrared and Raman Spectra of Polyatomic Molecules*; D. van Nostrand: Princeton, NJ, 1968.
(43) Kester, D. R.; Duedall, I. W.; Connors, D. N.; Pytkowicz, R. M. *Limnol. Oceanogr.* **1967**, *12*, 176.
(44) Rowland, B.; Kadagathur, N. S.; Devlin, J. P. *J. Chem. Phys.* **1995**, *102*, 13.
(45) Kittel, C. *Introduction to Solid State Physics*, 6th ed.; Wiley: New York, 1986.
(46) Agron, P. A.; Busing, W. R. *Acta Crystallogr.* **1985**, *C41*, 8.
(47) Agron, P. A.; Busing, W. R. *Acta Crystallogr.* **1986**, *C42*, 141.
(48) Leclaire, P. A.; Borel, M. M. *Acta Crystallogr.* **1977**, *B33*, 1608.
(49) Lad, R. A. *Surf. Sci.* **1968**, *12*, 37.
(50) Barraclough, P. B.; Hall, P. G. *Surf. Sci.* **1974**, *46*, 393.
(51) Smart, R. St. C.; Sheppard, N. *J. Chem. Soc., Faraday Trans. 2* **1976**, *72*, 707.
(52) Dai, D. J.; Peters, S. J.; Ewing, G. E. *J. Phys. Chem.* **1995**, *99*, 10299.
(53) Griffiths, P. R.; Fuller, M. P. *Adv. Infrared Raman Spectrosc.* **1982**, *10*, 63.
(54) TeVrucht, M. L. E.; Griffiths, P. R. *Appl. Spectrosc.* **1989**, *43*, 1293.
(55) DeMore, W. B.; Sander, S. P.; Golden, D. M.; Hampson, R. F.; Kurylo, M. J.; Howard, C. J.; Ravishankara, A. R.; Kolb, C. E.; Molina, M. Chemical Kinetics and Photochemical Data for Use in Stratospheric Modeling. Evaluation No. 11; JPL Publication 94-26, 1994.
(56) Sverdrup, G. M.; Kuhlman, M. R. *Stud. Environ. Sci.* **1980**, *8*, 245.
(57) Sakamaki, F.; Hatakeyama, S.; Akimoto, H. *Int. J. Chem. Kinet.* **1983**, *15*, 1013.
(58) Pitts, J. N., Jr.; Sanhueza, E.; Atkinson, R.; Carter, W. P. L.; Winer, A. M.; Harris, G. W.; Plum, C. N. *Int. J. Chem. Kinet.* **1984**, *16*, 919.
(59) Svensson, R.; Ljungström, E.; Lindqvist, O. *Atmos. Environ.* **1987**, *21*, 1529.
(60) Jenkin, M. E.; Cox, R. A.; Williams, D. J. *Atmos. Environ.* **1988**, *22*, 487.
(61) Bambauer, A.; Brantner, B.; Paige, M.; Novakov, T. *Atmos. Environ.* **1994**, *28*, 3225.
(62) Mertes, S.; Wahner, A. *J. Phys. Chem.* **1995**, *99*, 14000.
(63) Wan, J. K. S.; Pitts, J. N., Jr.; Beichert, P.; Finlayson-Pitts, B. J. *Atmos. Environ.* **1996**, *30*, 3109.
(64) Plumb, R. C.; Edwards, J. O. *J. Phys. Chem.* **1992**, *96*, 3245.